Polarization dependence of optically-driven elastomer mechanics.

D. Corbett and M. Warner

Cavendish Laboratory, University of Cambridge, Madingley Road, Cambridge CB3 0HE, U.K.

(Dated: September 24, 2008)

We model how polarized and unpolarized light can cause mechanical response in nematic and related photo-elastomers. The reduction of order by heating and the consequential large strains that are known from nematic elastomers can alternatively be caused by light-induced bending of rodlike dye molecules which then equally reduce the order of their nematic hosts. While there is no mechanical response to heating of polydomain elastomers, mechanical response to light is possible by the selective absorption of light according to how domains are aligned with respect to the polarization direction or with respect to the propagation direction in the case of unpolarized light. We find large contractions or elongations, depending on the nature of polarization. The responses are non-monotonic with light intensity.

PACS numbers: 61.41.+e, 83.80.Va, 82.35.Ej, 78.20.Hp

I. INTRODUCTION

Mechanical response can be optically-induced in monodomain liquid-crystalline networks with molecular rods that undergo a *trans-cis* isomerization on absorbing an appropriate photon. Response is huge in nematic elastomers [1–4] where, as in all rubbers, elastic moduli are small. Smaller, but still very useful responses in nematic glasses exist [5–9] where moduli are large. We concentrate on photo-mechanical response in elastomers, which can be understood by first considering their conventional, thermally-induced contractions when they are nematic monodomains. The contractions can be huge [10, 11], up to a factor of 4 or more: heating reduces the orientational order and hence the shape anisotropy of the distribution of the polymer chains making up the elastomeric network. Macroscopic strain then follows the network chains' shape change. In section II C we sketch the derivation of such shape change. Schematically, figure 1(a) shows this shape change in response to order change.

Light can also reduce the order parameter in nematics when dye molecules (chromophores, for example contain-
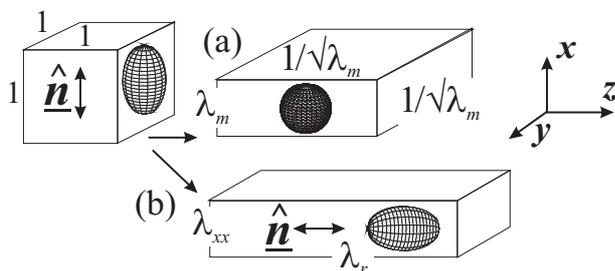

FIG. 1: An initially unit, cubical nematic elastomer (a) contracts on loss of order. The prolate spheroid characterizing the distribution of chains becomes spherical; (b) contracts along the original director, and elongates along the new, upon rotation by 90° of the director and thus of shape distribution.
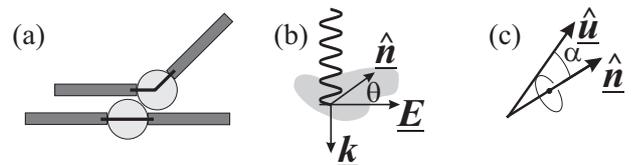

FIG. 2: (a) *trans* and *cis* (bent) forms of a dye rod with a central azo unit. Parallel ordering of the remaining rods is hindered by the bent species. (b) a polydomain elastomer illuminated by light polarized along the $\underline{E}$ direction (c) a test rod, direction $\underline{\hat{u}}$, in a region with director currently along $\underline{\hat{n}}$

ing azo-benzene) are present. Chromophores are often rod-like in their ground (*trans*) state. Photon excitation yields a bent *cis* state, see fig. 2(a), and nematic order is reduced, analogously to the thermal case, as the dye is converted. In a nematic network, a mechanical strain then follows [1]. In the dark, the order parameter recovers its original value as bent molecules decay back to their straight *trans* conformation and hence the strain is reversed. Another route to recovery is the stimulation, by light of another color, of the *cis* to *trans* transition which offers even greater speed and control.

We shall also consider another important mechanism for photo-mechanical distortion, that of director rotation rather than order change. It is known when nematic elastomers are extended perpendicular to their initial director that the director is induced to rotate [12]. Since the (on average) long direction of the chains (along the director) is rotated, then the network naturally extends in this direction, see figure 1(b). Indeed the stresses associated with strains imposed perpendicular to a director which then rotates are known [13] to be much lower than the stresses arising when there is no rotation or when the elastomer is in the isotropic phase. Here our theory suggests an inverse effect that under illumination the nematic free energy can, at least at low light intensity, be kept lower by rotating the director rather than reducing the magnitude of the nematic order. There is then an as-

sociated strain where the network's shape follows that of the rotating distribution of anisotropic chains. We shall predict complex photo-mechanical response and find that director rotation initially dominates over the reduction of orientational order as the cause of mechanical strain.

The photo-response of polydomain systems appears to prove that light actuation is in fact an optical effect rather than simply light delivering heat in another way: Ikeda and Yu *et. al.* [5, 6] induced a glassy polydomain network to contract along the polarization direction of the incident light. Harvey and Terentjev [14] fixed the length of a polydomain nematic elastomer and instead followed the build up of stress depending on the direction the polarization of light with respect to the clamping direction. No thermal actuation of polydomain systems is possible since no unique direction exists. If one assumes that optical effects are simply due to heat being preferentially delivered to domains aligned with the polarization, then difficulties also arise: Any unique direction associated with incident polarized light is also lost if one assumes that heat, released on the back-decay from the *cis* excited to *trans* ground state in regions aligned with the polarization direction, is then transferred quickly to other regions. The assumption of short times is reasonable: Hon *et al* [15] obtained $D \approx 1.5 \times 10^{-7} \mathrm{m}^2/\mathrm{s}$ for the heat diffusion coefficient of a side-chain nematic elastomer, while Broerman *et al* [16] obtained $D \approx 1.1 \times 10^{-7} \mathrm{m}^2/\mathrm{s}$ for an isotropic, silicone-based elastomer. Assuming director correlation over $l \lesssim 1\mu m$ we estimate the characteristic time for heat to diffuse to another region to be $\sim l^2/D = 10\mu$s, much shorter than observed mechanical response times.

The polarization specificity of the contractions of these polydomain samples offers much richer behavior than that of monodomains. In fact the polarization-specific response of the Ikeda networks was photo-curling and could be directed along any axis desired, useful for complicated actuation. Sometimes photo-contraction manifests itself as photo-curling of a cantilever or sheet – when light attenuation is appreciable through the thickness of the sample, it gives rise to strains greater near the front face than those near the rear. However, here we only consider samples thin enough compared with both the absorption and depolarization lengths, such that both the contraction is uniform and the light remains polarized. Our examination of uniform contraction mechanisms will be important to subsequent studies of curling polydomain cantilevers.

Suggested applications of elastomer photo-elasticity include micro- and nano- actuation by curling cantilevers [17], microfluidic valves and pumps by optically writing localized topographical structures in elastomer films [17, 18], and artificial muscles [19]. Our predictions of elongation along the propagation direction for unpolarized light falling on polydomain elastomers may be of particular importance for the writing of localized structures by light beams on elastomeric films.

We limit our modeling to the photo-response of poly-domain *elastomers*, rather than glasses. It is probable that only the former have directors sufficiently mobile in the solid state to rotate in response to light or imposed strains. Initial modeling [20], of weakly crosslinked polydomain nematic elastomers illuminated with polarized light, yielded a sharp initial contraction as directors rotated away from the optical electric field, eased by a global strain that was a compromise between domains with rotation differing according to their initial orientation with respect to this electric field. Accordingly negative optical anisotropy must be induced in the network. We shall explore elsewhere the ramifications for NMR which gives much more detail of the induced molecular distributions. We additionally predicted that the uniform photo-strain is non-monotonic with the intensity of the incident light. At high light intensity domains suffer the same *trans* to *cis* conversion and hence suffer the same reduction in order, irrespective of their initial orientation. With all domains equivalent, this situation is equivalent to just heating a polydomain elastomer. Because there is no longer a favored direction, the sample recovers its original shape even though the constituent domains have individually changed their nematic order. We shall see this non-monotonicity prediction retained for unpolarized light incident on a polydomain elastomer. As well as dealing here with several polarization and polydomain types, we also extend our modeling to strongly crosslinked elastomers which offer certain qualitative distinctions from our earlier analysis.

The non-monotonicity of the response with intensity could even lead to a reversal of the sign of cantilever curvature. When the incident light intensity is high enough that the photo-strain at the upper surface vanishes, but where there is contraction lower down, then the beam will curve away from rather than towards the light.

II.   A NON-LINEAR MODEL OF POLYDOMAIN ELASTOMER PHOTO-RESPONSE

The situation we first model is shown in fig. 2. Plane polarized light propagating in the $\underline{k}$ direction is incident normally on a thin polydomain liquid crystal elastomer (LCE). A region with current director $\hat{\underline{n}}$ is shown; we neither discuss the origin of domains, nor require their length scale (typically microns), in what follows. We model an elastomer with initially random directions for domains. At each point the extent of photo-reactions depend on the angle between the local director and the electric field. The strain however we will take to be global, as we discuss below. Clearly mechanical effects globally can only have the polarization direction $\underline{E}$ as the unique direction. Having set up our model with the example of polarized light, we will later consider incident unpolarized light, where the unique mechanical axis will instead become $\underline{k}$. Finally we consider the photo-mechanical response of cholesteric elastomers to unpolarized light propagating along the helix axis.

A. Intensity and angular dependence of isomer concentrations

The rod-like character of molecules is responsible for the orientational order of the nematic state. To examine the stability of the nematic state, we therefore first determine how their number changes as a result of irradiation. Consider a total number density n_n of nematogenic rods, of which a number density n_p are photo-responsive nematogens (giving a fraction $A = n_p/n_n$). In the domain shown in Fig. 2(b) a photo-rod is described by a unit vector $\underline{\hat{u}}$ along its long axis. In the simple case of chromophores also with $\underline{\hat{u}}$ as the direction of their active bonds, the probability of photon absorption by a rod depends on the intensity along its axis, $(\underline{E}{\cdot}\underline{\hat{u}})^2$. The rate per unit volume of photo-induced *trans-cis* reactions is hence $\Gamma \left\langle (\underline{E} \cdot \underline{\hat{u}})^2 \right\rangle n_t(t)$, where Γ is a constant, and $n_t(t)$ is the current number density of *trans* nematogens at time t. The local thermodynamic average $\langle\,\rangle$ is taken over photo-rods in the region with $\underline{\hat{n}}$. The thermal back reaction rate is $n_c(t)/\tau = (n_p - n_t(t))/\tau$, where $n_c(t)$ is the number density of photo-rods converted to the *cis* state (thus $n_t + n_c = n_p$). The *cis* state's mean lifetime is τ, which depends on temperature in the thermal case and on light intensity when recovery is optically stimulated. We assume that the *cis* rods have no orientational order and are randomized when they reenter the *trans* population on decay. In the steady state the forward and backward rates match and the fractional *cis* population n_c is

$$\frac{n_c}{n_p} = \frac{\Gamma\tau \left\langle (\underline{E} \cdot \underline{\hat{u}})^2 \right\rangle}{1 + \Gamma\tau \left\langle (\underline{E} \cdot \underline{\hat{u}})^2 \right\rangle}. \qquad (1)$$

We have assumed first order dynamics, that is, the forward and backward reactions depend linearly on n_t and n_c respectively, and also that the rates Γ and $1/\tau$ are unaffected by mechanical strain, nematic order etc. We must now calculate the average $\left\langle (\underline{E} \cdot \underline{\hat{u}})^2 \right\rangle$, which can be written as $Tr[\langle \underline{E}\,\underline{E} \rangle_E \langle \underline{\hat{u}}\,\underline{\hat{u}} \rangle_{\hat{u}}]$ where $\langle X \rangle_E$ indicates an average over the orientations of the electric field while $\langle X \rangle_{\hat{u}}$ indicates an average over the orientations of the photo-rods. Assuming the electric field is linearly polarized along the z-direction gives $\langle \underline{E}\,\underline{E} \rangle = E^2 \underline{z}\,\underline{z}$. The traceless order parameter tensor for the (uniaxial) photo-rods is:

$$S_{ij} = \left\langle \tfrac{3}{2}u_i u_j - \tfrac{1}{2}\delta_{ij} \right\rangle_{\hat{u}} = S\left(\tfrac{3}{2}n_i n_j - \tfrac{1}{2}\delta_{ij} \right) \qquad (2)$$

where S is the scalar uniaxial order parameter and $\underline{\hat{n}}$ is the director. Using eqn (2) for $\langle u_i u_j \rangle_{\hat{u}}$ we obtain:

$$\left\langle (\underline{E} \cdot \underline{\hat{u}})^2 \right\rangle = \tfrac{1}{3}E^2(1 + 2\underline{z} \cdot \underline{\underline{S}} \cdot \underline{z}). \qquad (3)$$

In general photo-rods which lie on a cone at a fixed angle with respect to the principal director $\underline{\hat{n}}$ will be differently aligned with the electric field (unless $\underline{E}$ and $\underline{\hat{n}}$ are parallel), thus such rods are differentially depleted and we should expect illumination to induce biaxiality. However, we assume that the angular diffusion rate of rods

is rapid, thus each photo-rod explores all angles around the director $\underline{\hat{n}}$ between excitation events. We thus ignore biaxiality. With this simplification eqn (3) can be expressed as:

$$\left\langle (\underline{E}.\underline{u})^2 \right\rangle = \tfrac{1}{3}I[1 + 2SP_2(\cos\theta)], \qquad (4)$$

where $P_2(\cos\theta)$ is the second Legendre polynomial, the intensity $I = E^2$ and θ is the angle between the director $\underline{\hat{n}}$ of the domain and the z-direction. Inserting this result into eqn (1) and normalising to the total number of all nematogens, one obtains the fractional number of *cis* molecules

$$\phi(S, I, \theta) = A\frac{I[1 + S(3\cos^2\theta - 1)]}{3I_c + I[1 + S(3\cos^2\theta - 1)]}. \qquad (5)$$

A characteristic light intensity has arisen from the balance of the forward (ΓI) and reverse ($1/\tau$) isomerization rates, that is $I_c = 1/\Gamma\tau$ [20]. We reduce light intensities by I_c, thus $\tilde{I} = I/I_c$. Measurement of n_c/n_p in isotropic polymers [21] suggests $\tilde{I}$ can be as large as 15, while timescales for attaining photo-equilibrium range from minutes to seconds, depending upon chemistry and stimulation of back-reactions. This quantity also determines the dynamics of non-linear light absorption and has been observed in experiments [22] to take much higher values than those of Eisenbach.

Since they are bent, we take the *cis* species to lack any nematicity. Indeed they dilute the ordering power of the remaining both non-photo and photo (*trans*) rods. The full difficulty of the problem can now be seen: in the expression (5) for ϕ, the order parameter S itself depends on ϕ since this dilution will enter the free energy, the minimization of which determines S. The free energy is not simply the standard nematic contribution familiar from conventional liquid crystals, but also the nematic rubber elastic free energy, and both contributors depend on the (changing) angle of the local director. It is thus instructive to see how ϕ changes with both intensity and angle of domain. The *cis* concentration in the low illumination limit, $\tilde{I} \ll 1$, is $\phi \to \tfrac{1}{3}\tilde{I}A(1 + 2SP_2(\cos\theta))$. Note that even domains at right angles to the polarization, with $\theta = \pi/2$ and thus $P_2(\cos\theta) = -1/2$, have some *cis* concentration induced if $S < 1$ because not all rods in the domain are perpendicular to $\underline{E}$ if the order is not perfect. At very high intensity, $\tilde{I} \gg 1$, all photo-rods are bent, $\phi \to A$, and all domains are bleached, irrespective of angle. Thus eventually, perpendicular domains are also bleached, except in the unphysical case of those with perfect underlying order, $S = 1$. It is the eventual bleaching of all regions that causes the polydomain system to lose overall mechanical response when light is intense: if all domains have the same ϕ, their mechanical fate must be the same. The lack of a preferred direction implies zero strain for a polydomain system, just as one obtains no strain on heating such a system to another state of order.

B. Mean field theory

A mean-field theory for nematics was first proposed by Maier and Saupe [23]. The simplest Hamiltonian to describe uniaxial nematic ordering arises after azimuthal averaging about $\hat{n}$ (the free angle in Fig 2(b)):

$$H = -\frac{1}{2}\sum_{i\neq j} J_{ij} P_2(\cos\alpha_i) P_2(\cos\alpha_j), \qquad (6)$$

where α_i is the angle of the long axis of the ith nematogen with respect to the director $\hat{n}$, J_{ij} represents the interaction potential between the ith and jth rod and the sum is taken over all pairs of nematogens. Maier and Saupe (M-S) assumed that the interacting potential arose from anisotropic van der Waals forces, but the precise form of J_{ij} is not important here. We follow the M-S approach, but with vital modifications to deal with populations of rods changing on illumination by amounts dependent upon the mean order.

To determine the mean-field free energy one adopts a variational approach based upon the inequality:

$$F \leq F_0 + \langle H - H_0 \rangle_0 \qquad (7)$$

where F_0 is the free energy evaluated using a trial Hamiltonian H_0, and F is that by using H, and $\langle \ldots \rangle_0$ denotes an average from H_0. For the trial Hamiltonian we assume an ensemble of non-interacting nematogens placed within an as yet undetermined field h, giving $H_0 = -h\sum_i P_2(\cos\alpha_i)$ and $F_0 = -k_B T \sum_i \ln(Z_0(h/k_B T))$ with the partition function Z_0 associated with the trial Hamiltonian given by:

$$Z_0 = \int_0^1 d(\cos\alpha)\exp\left[hP_2(\cos\alpha)/k_B T\right]. \qquad (8)$$

The free energy f_{MS} per unit volume of a M-S liquid crystal is thus bounded by:

$$F \leq n_n\left[-k_B T \ln Z_0(h/k_B T) + hS - \tfrac{1}{2}JS^2\right], \qquad (9)$$

where n_n is the number density of nematogens, J is a coupling constant determined from the J_{ij} above and $S = \langle P_2(\cos\alpha)\rangle_0$ is the scalar order parameter. We now sketch the familiar liquid crystal case since there are significant deviations from this for photo-elastomers. Minimizing the right hand side of (9) with respect to h gives $S = k_B T\partial(\ln Z_0)/\partial h \equiv g_0(h/k_B T)$. and thus:

$$\frac{h}{k_B T} = g_0^{-1}(S). \qquad (10)$$

See Appendix A for more details about $g_0(x)$ and its inverse. Minimizing (9) now with respect to S gives $h = JS$, thus giving $S = (k_B T/J)g_0^{-1}(S)$, which can be inverted to give the Maier-Saupe self-consistency equation $S = g_0(JS/k_B T)$ for the order parameter. The scaling of the coupling constant J with n_n is important;

since the initial Hamiltonian H describes pair-wise interactions we should expect it to scale quadratically with the number density of nematogens n_n. In eqn (9) we have extracted one factor of n_n as a pre-factor, thus J is expected to scale linearly with n_n.

The photo-elastomers we model contain several complicating factors. First, the free energy also has the elastic response of the elastomer which introduces additional S dependence and makes the result $h = JS$ from $\partial f/\partial S = 0$ no longer valid. However, relation (10) from $\partial f/\partial h = 0$ does remain valid. Secondly, illumination produces a population of *cis* rods within each domain, which dilute the nematic ordering tendency of the remaining rods. Now the number density of nematogens n_n is reduced to $n_n(1-\phi)$: eqn (9) becomes:

$$\begin{aligned}f_{LC} = {} & n_n k_B T(1-\phi)\big\{g_0^{-1}(S)S - \\ & - \ln Z_0(g_0^{-1}(S)) - \tfrac{1}{2}(1-\phi)\frac{J}{k_B T}S^2\big\}, \quad (11)\end{aligned}$$

where we have replaced $h/k_B T$ from eqn (10) and we recall from eqn (5) that ϕ is a function of both S and the angle θ between the domain considered and the electric field. By itself, the nematic free energy above resembles that of a nematic liquid with its interactions diluted by the presence of non-nematic, bent rods. There is no entropy of mixing since in a network the nematic elements are permanently linked and do not mix freely. Appendix B considers the consequences of this free energy in isolation since the coupling of order with concentration of *cis* give highly non-trivial variation of order with temperature and polarization of illumination. The distinction between the global order parameter $Q = (1-\phi)S$ as measured by birefringence and that of the participating nematogens S as measured by NMR is also discussed there.

C. Elastomer deformation free energy

Elastomers are networks of polymeric strands with shapes that are induced to change by the ordering of pendant or integral nematogenic rods. Classical Gaussian rubber elasticity generalizes to a nematic rubber-elastic free energy density [24, 25]

$$f_{EL} = \tfrac{1}{2}\mu\mathrm{Tr}\left[\underline{\underline{\lambda}}\cdot\underline{\underline{l}}_0\cdot\underline{\underline{\lambda}}^T\cdot\underline{\underline{l}}^{-1}\right] + \tfrac{1}{2}\mu\ln\left[\frac{\det[\underline{\underline{l}}]}{\det[\underline{\underline{l}}_0]}\right] \qquad (12)$$

in which $\mu = n_s k_B T$ is the shear modulus, with n_s the number density of network strands and $\underline{\underline{\lambda}}$ the deformation gradient tensor. The bulk modulus of elastomers is typically $\sim 10^4\mu$. They consequently deform at constant volume, constraining $\underline{\underline{\lambda}}$ to have unit determinant. The remaining tensors $\underline{\underline{l}}_0$ and $\underline{\underline{l}}^{-1}$ are the shape and inverse shape tensors defining the Gaussian distribution of uniaxial nematic polymer chains before and after illumination. They are characterized by the anisotropy direction,

initially $\hat{n}_0$ and rotating to $\hat{n}$, and the degree of order, initially S_0 and relaxing to a new S since $\phi \neq 0$. Within the freely jointed rod model we assume the polymer chains between two cross-links consists of a sequence of connected rods, which can rotate freely about their points of connection. The *trans* and photo-inert nematogens have a step-length a, while the *cis* nematogens have b. We further assume that the orientational distribution of the *cis* nematogens is isotropic, while the photo-inert and *trans* molecules are uniaxially aligned. With these assumptions the step-length tensors take their usual form:

$$\underline{\underline{l}}_0 \ = \ l_\perp^0 \underline{\underline{\delta}} + \left(l_\| - l_\perp^0 \right) \hat{n}_0 \hat{n}_0, \qquad (13)$$

$$\underline{\underline{l}}^{-1} \ = \ \frac{1}{l_\perp} \underline{\underline{\delta}} + \left(\frac{1}{l_\perp} - \frac{1}{l_\|} \right) \hat{n}\,\hat{n}, \qquad (14)$$

where the various step lengths are given by

$$l_\perp^0 \ = \ a(1 - S_0)\,; \qquad l_\|^0 = a(1 + 2S_0) \qquad (15)$$

$$l_\perp \ = \ a\left[(1-\phi)(1-S) + \phi(b/a)^2 \right] \qquad (16)$$

$$l_\| \ = \ a\left[(1-\phi)(1+2S) + \phi(b/a)^2 \right] \qquad (17)$$

Appendix C derives these results.

In a freely jointed model for main-chain elastomers the order parameter of the nematogens S would be coincident with that of the chain backbone S_B. If instead the nematogens are pendant to the polymer backbone these two order parameters would in general differ. The pendant rods order and then indirectly induce order in the backbone. Experimentally it has been observed by Finkelmann *et. al.* [26] that for prolate side-chain nematic elastomers S_B is proportional to S, thus the scalar order parameters within the step-length tensors should include a constant of proportionality when describing side-chain elastomers. For this work we ignore this distinction.

The shape tensors set the scale for spontaneous deformations: Heating a *monodomain* initially with order S_0 directed for concreteness along $\underline{n}_0 = \underline{z}$ to the isotropic state ($S \to 0$ in $\underline{\underline{l}} \to a\underline{\underline{\delta}}$ above), eqn (12) predicts that the elastomer would suffer a uniaxial contraction of $\lambda_m = \left(l_\perp^0 / l_\|^0 \right)^{1/3} = ((1 - S_0)/(1 + 2S_0))^{1/3} \sim 0.56$ [25] for the initial order parameter of $S_0 = 0.615$ adopted in our illustrations. [One inserts into eqn (12) a uniaxial deformation identical to $\underline{\underline{\lambda}}_E$ in (18) below for $\underline{\underline{\lambda}}$ along with $\underline{\underline{l}}_0$ and $\underline{\underline{l}}$ given above, the latter with $\phi = 0$ and $S = 0$.]

If cooling down from the isotropic to nematic phase there would instead be an elongation of $1/\lambda_m = 1.78$. Separate measurements [26] of the order parameter $S(T)$ (optically) and the spontaneous distortion confirm the freely-jointed rod model connection $\lambda_m(T) = ([(1 + 2S_0)/(1 - S_0)][(1 - S)/(1 + 2S)])^{1/3}$ where this contraction is associated with changes in order from S_0 to a finite S. In practice even nearly ideal nematic elastomers do not suffer the M-S jump in order parameter (and hence in strain) at the transition temperature T_{NI} because of non-ideal additions to eqn (12), in effect internal fields. These effects are widely discussed in the literature; see a summary in [25] and a modern discussion plus experimental NMR analysis [27].

The essential anisotropy that determines λ_m also determines the shape change of a monodomain that would occur when the director is rotated by $90°$ with a change in the order. One proceeds as above, but with an $\underline{\underline{l}}$ having $S = S_0$, $\phi = 0$ and with $\underline{n}$ rotated to being along x rather than remaining along z that one associates with $\underline{n}_0$. The $\underline{\underline{\lambda}}$ now has as its diagonal elements λ_r, $1/(\lambda_r \lambda_{zz})$, λ_{zz} which is volume-preserving and represents an elongation of λ_r along x. Simple minimization over λ_{zz} and λ_r [25] yields $\lambda_r = \left(l_\|^0 / l_\perp^0 \right)^{1/2} \to 2.38$ for $S_0 = 0.61$. Note that this elongation is greater than the elongation $\left(l_\|^0 / l_\perp^0 \right)^{1/3}$ associated with increasing order from the isotropic to nematic state – redirecting an already elongated distribution of polymers has a much greater effect, see figure 1.

We now decide how to adopt a deformation gradient tensor for the illuminated polydomain elastomer: Boundaries between individual domains are subject to several constraints. Mechanical equilibrium requires the stress tensor be divergence free, in particular in its variation across boundaries. Geometric requirements place compatibility constraints upon the deformation gradient tensor $\underline{\underline{\lambda}}$, which in the present case must also preserve volume. Similar constraints arise when modeling polycrystalline metals. We return to the question of compatibility in discussing the cholesteric case. Satisfying both constraints is in general difficult and one usually adopts one of two limiting forms. In the Sachs limit all domains suffer the same stress, thus satisfying the mechanical requirements but in general failing to meet the compatibility requirements. In the Taylor limit all domains suffer the same deformation, thus meeting the compatibility requirements but not in general obeying mechanical equilibrium. For small strain elasticity these two limits form lower and upper bounds on the true free energy of the system. It is this second limit of uniform strain that we adopt here, albeit in systems with large strains. We take simple, uniaxial (about $\underline{E}$ or $\underline{k}$ – hence the labels), deformation gradients $\underline{\underline{\lambda}}$:

$$\underline{\underline{\lambda}}_E = \begin{pmatrix} \frac{1}{\sqrt{\lambda}} & 0 & 0 \\ 0 & \frac{1}{\sqrt{\lambda}} & 0 \\ 0 & 0 & \lambda \end{pmatrix} \qquad \underline{\underline{\lambda}}_k = \begin{pmatrix} \lambda & 0 & 0 \\ 0 & \frac{1}{\sqrt{\lambda}} & 0 \\ 0 & 0 & \frac{1}{\sqrt{\lambda}} \end{pmatrix} \qquad (18)$$

that also conserve volume, $\det(\underline{\underline{\lambda}}) = 1$. The first is for polarized light, where $\underline{E}$ is the unique direction, the second for unpolarized light where $\underline{k}$ is the unique direction. In effect we assume that the global strain we must have holds locally as well. The latter $\underline{\underline{\lambda}}$ will be augmented with compatible strains in the cholesteric case, section III C, where we elaborate on this requirement.

D. Other additions to the free energy

The wall energy that exists between the domains may change as a result of elastic distortions. Approximately, the elastic energy of a domain of characteristic size ξ_D is $\sim \mu\xi_D^3$. The wall energy between the domains has two contributions, a Frank term owing to the changing director and gradients of the order parameter, and an elastic term since the deformation gradient in the wall region is not able to adopt its optimal value. These two contributions are added and optimized over. The minimum occurs when both contributions are equal, giving us a length scale $\xi_N = \sqrt{K/\mu} \approx 10^{-8}$m for the wall thickness where $K \sim 10^{-11}$N is a Frank constant and $\mu \sim 10^5$Pa. This length is known as the nematic penetration depth [25] and arises whenever Frank and rubber elastic effects compete. The energy per unit area of wall that arises is $\gamma \sim \sqrt{K\mu}$ and the wall energy of a domain is roughly $\gamma\xi_D^2$. The ratio of the energies is $\gamma/(\mu\xi_D) = \xi_N/\xi_D$. A typical domain size is $\xi_D \approx 1\mu$m [28], thus the wall energy is roughly 100 times smaller than the elastic energy of each domain. We therefore choose to ignore this contribution to the free energy.

E. Overall free energy

Inserting $\underline{\lambda}$ into f_{EL}, eqn (12), and adding this energy to f_{LC} from eqn (11) gives the local free energy $f_{EL} + f_{LC}$. The polydomain sample initially consists of an isotropic distribution of domains, each with order parameter S_0. Domains are labeled by θ_0, their initial director orientation relative to the electric field. At a given λ, a domain initially at θ_0 will move to a new value θ dependent on both θ_0 and λ; thus $\theta = \theta(\theta_0, \lambda)$. Equally the order parameter in the domain will change from its initial value S_0 to a new value S which depends on θ_0 and λ, thus $S = S(\theta_0, \lambda)$. To calculate the total free energy, f_{tot}, of the material we must then sum over all initial orientations of the domains, thus:

$$f_{tot}(\lambda) = \int_0^{\frac{\pi}{2}} (f_{LC}(\theta_0) + f_{EL}(\theta_0)) \sin\theta_0 d\theta_0. \quad (19)$$

The total free energy f_{tot} is a function of the deformation λ, and a functional of the order parameter $S(\theta_0, \lambda)$ and the director orientation $\theta(\theta_0, \lambda)$. For each value of θ_0 we minimize the integrand in eqn (19) over θ and S, then sum over all domains, and finally minimize over λ. Since each domain suffers the same compromise $\underline{\lambda}$, they are in general at a shape suboptimal for their current conditions. Such distortions act in effect as powerful external fields. As with all nematics, a strong enough field can induce supercritical behavior. Here they can eliminate jumps in the order parameter of LCEs as they are heated to isotropy.

We summarize the quantities appearing within the total free energy density, eqn (19), their physical meaning

and realistic values.

$\tilde{J} = J/k_BT$ – scaled Maier-Saupe interaction parameter, which sets the initial value of the order parameter within each domain. Within bare MS theory the isotropic-nematic transition occurs for $\tilde{J} = 4.54$. In all the work presented here we set $\tilde{J} = 5$, which gives $S_0 = 0.61$. In relation to the nematic-isotropic transition temperature T_{NI} this choice corresponds to an operating temperature T_0 given by $T_0 = (4.54/5)T_{NI} = 0.91T_{NI}$.

$\tilde{\mu} = \mu/(n_nk_BT)$ – is the shear modulus reduced by the natural energy scale appearing in eqn (11) for the nematic energy density. Thus in these units the shear modulus is given by the ratio of the number density of network strands to the number density of nematogens, and is thus a measure of the cross-linking strength. Values for elastomers range from roughly 0.1 to 0.02.

$\tilde{I} = I/I_c$ – the reduced intensity which corresponds to the optical intensity, divided by the intensity I_c which is a material constant of the elastomer film under consideration. Results from Eisenbach [21] indicate that values up to $\tilde{I} \approx 15$ are easily accessible, and those from Serra and Terentjev [22] suggest values ~ 80.

A – There are two types of nematogens, photo-active and photo-inert. The fraction of nematogens which are photo-active is given by A. We shall take $A = 1/6$ throughout this work, that is, there are five photo-inert nematogens for each photo-active one. Here we make the additional simplification that the ordering of the inert nematogens and that of the *trans* photo-rods is the same.

III. RESULTS

We present results showing the equilibrium deformation gradient λ as a function of the incident reduced intensity $\tilde{I}$ for three separate cases: (i) polarized light upon a polydomain elastomer (ii) unpolarized light upon the same sample, (ii) unpolarized light on a planar distribution of domain directors, i.e. a two-dimensional equivalent of a polydomain that is perhaps realizable as a cholesteric elastomer. In each of these three separate cases, we present results for a strongly cross-linked sample with $\tilde{\mu} = n_s/n_n = 1/10$ and more weakly cross-linked sample with $\tilde{\mu} = 1/50$.

A. Incident polarized light

A deformation uniaxial with $\underline{E}$ is inserted into the elastic energy. We do not give details of how the energy can first be minimized with respect to λ given the initial and current director directions and the initial and current order parameters – see [25] for examples of how this is done, and the cholesteric section below.
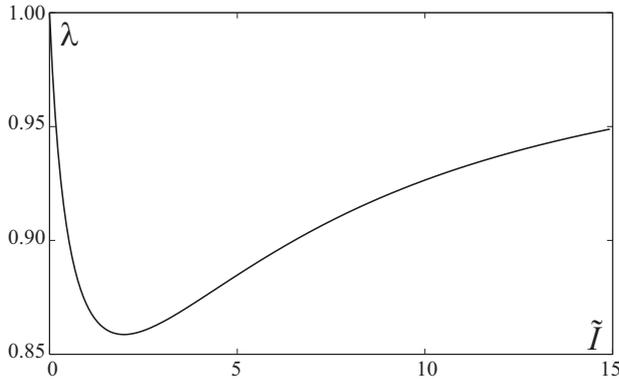
FIG. 3: The global z-contraction λ against reduced intensity of polarized light $\tilde{I}$ for a strongly cross-linked elastomer with $\tilde{\mu} = 1/10$ $T = 0.91 T_{NI}$, $S_0 = 0.61$.

1.   Strong Cross-linking

Figure 3 shows the photo-contraction $\lambda(\tilde{I})$ as a function of the reduced light intensity $\tilde{I}$ for a ratio of network strands to rods $\tilde{\mu} = n_s/n_n = 1/10$. The fraction of rods that are photo-active is $A = 1/6$ and the initial order parameter $S_0 = 0.615$. Following Eisenbach [21] we have taken the ratio of step lengths appearing in eqn (16-17) to be $b/a = 5.5/9$. The most prominent feature of the curve is that it is non-monotonic; initially λ decreases rapidly as $\tilde{I}$ increases, but beyond $\tilde{I} \approx 2$ the trend reverses and λ begins to increase as $\tilde{I}$ increases further. The biggest contraction, $\lambda = 0.86$, corresponds to $\tilde{I} \sim 2$. This should be compared with the thermal contraction expected when a nematic monodomain with the same S_0 is heated to isotropy, which gives $\lambda_T = 0.56$ as discussed previously. Evidently we manage to recover approximately a third of the mono-domain contraction when illuminating the polydomain. In order to explain the behavior of the $\lambda(\tilde{I})$ curve it is instructive to plot the functions $\theta(\theta_0; \tilde{I}) - \theta_0$ (figure 4) and $S(\theta_0; \tilde{I})$ (figure 5) for various intensities. Focusing on the two plots for $\tilde{I} = 0.15$ we see that $\theta - \theta_0 \geq 0$ for all θ_0 (with equality for $\theta_0 = 0$ and $\theta_0 = \pi/2$), i.e. all domains have rotated away from the polarization direction. The nematic part of the free energy is minimized if domains are perpendicular to the electric field, this configuration also results in domains preserving more of their order. Rotation away from their initial orientations has an associated elastic energy penalty, which is partially vitiated through mechanical relaxation. The resulting λ reflects these rotations and corresponds to a compression along the electric field. It is interesting to note that for a narrow range of angles around $\theta_0 = \pi/2$ the order parameter increases, that is $S > S_0$. The overall contraction $\lambda < 1$ leads to an expansion $1/\sqrt{\lambda} > 1$ in the xy plane. This expansion acts as an aligning field for the domains around $\pi/2$ increasing their order parameter.

Increasing the intensity to $\tilde{I} = 1.05$, the situation is largely unchanged; the domains have rotated further
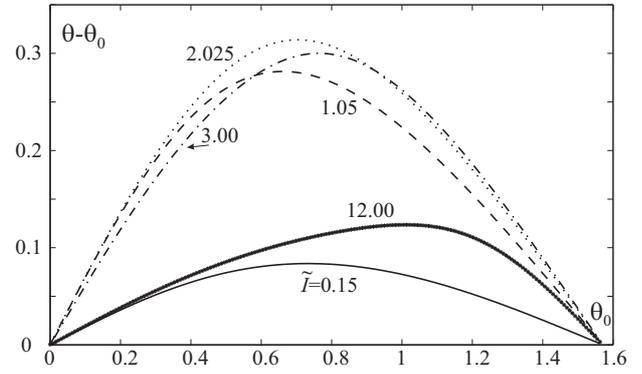

FIG. 4: The change in domain orientation, $\theta - \theta_0$ as a function of initial orientation θ_0 for various intensities of polarized light for an elastomer with $\tilde{\mu} = 1/10$.
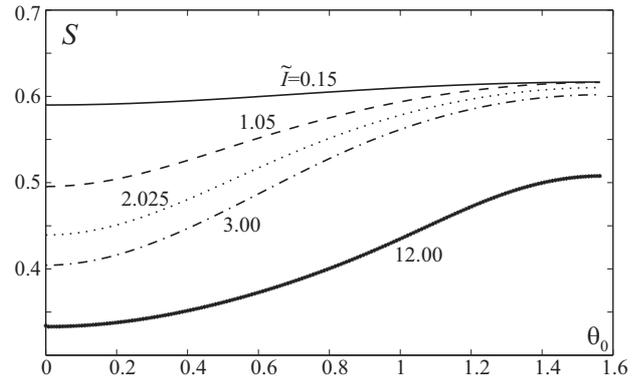

FIG. 5: The domain order parameter, S as a function of initial orientation θ_0 for various intensities of polarized light for an elastomer with $\tilde{\mu} = 1/10$.

from the polarization direction. Again there is a range of angles close to $\pi/2$ over which the order parameter increases. Those domains which remain close to $\underline{E}$ have suffered a larger reduction in S. Both effects, large rotations and larger reductions in order lead to a larger contraction along the electric field and hence a smaller value of λ. Similar comments apply for $\tilde{I} = 2.025$.

Further increasing the intensity to $\tilde{I} = 3$ changes things significantly. The order parameter is now less than S_0 for all domain orientations, even for those directed well away from $\underline{E}$. The optimal mechanical response for those domains perpendicular to $\underline{E}$ is thus a contraction (relative to their state at $\tilde{I} = 2.025$) along their own director. They would thus want to expand along the polarization direction. Conversely those domains close to $\underline{E}$ suffer a larger change in S and their optimal mechanical response is a contraction along $\underline{E}$. The overall deformation remains a contraction along $\underline{E}$, but we note the contraction is now smaller than it was for $\tilde{I} = 2.025$, i.e. the deformation λ is a non-monotonic function of the incident intensity. Inspection of the plot of $\theta - \theta_0$ for this intensity reveals that domains have started to rotate back towards their initial orientations. Finally increasing
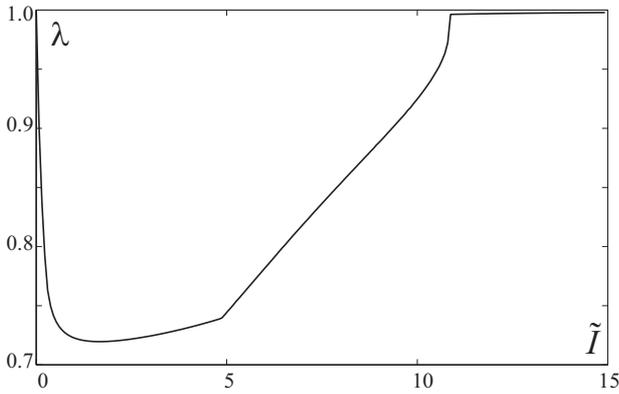
FIG. 6: Equilibrium deformation λ as a function of polarized light of reduced intensity $\tilde{I}$ for a weakly cross-linked elastomer with $\tilde{\mu} = 1/50$.

FIG. 7: Domain orientation θ as a function of the initial orientation θ_0 for various intensities of polarized light on an elastomer with $\tilde{\mu} = 1/50$.

FIG. 8: Domain order parameter S as a function of the initial orientation θ_0 for various intensities of polarized light on an elastomer with $\tilde{\mu} = 1/50$. Recall that the initial order was $S_0 = .615$.

the intensity substantially to $\tilde{I} = 12$, we see the trend of recovery of initial orientation and return of λ to 1 has continued. The order parameter has reduced yet further for all domains and there is still an overall contraction along $\underline{E}$. However, relative to the situation at $\tilde{I} = 3$ the system has expanded along $\underline{E}$, i.e. domains have rotated yet further back towards their initial orientations.

The non-monotonicity of the deformation gradient is perhaps obvious in hindsight. Taking the limit $\tilde{I} >> 1$ in eqn (5) we see that ϕ loses its dependence upon angle and tends towards the constant $\phi \rightarrow A$; at sufficiently high intensity all *trans* nematogens will be in their excited *cis* state. Since ϕ is constant, the nematic part of the free energy reverts to a standard Maier-Saupe form with a renormalized $J \rightarrow J(1 - A)$ and $n_n \rightarrow n_n(1 - A)$. The nematic energy no longer induces rotations away from $\underline{E}$, thus within the elastic free energy we must have $\theta = \theta_0$. Further, all domains will have the same order parameter $S = S_f$. Global isotropy and volume conservation then imply that $\lambda = 1$. In this limit it is not necessary that all domains are isotropic, but simply that they have the same, reduced order.

2. Weak Crosslinking

Increasing the number of nematogens per network strand, i.e. reducing the effective shear modulus in our model, results in much larger rotations away from the polarization direction. This weak linkage limit was treated in a preliminary analysis [20], but without considering the effect of the *cis* species on the step length tensors eqns (16-17). Comparison shows these refinements have little effect on the mechanics. Figure 6 shows the equilibrium deformation λ as a function of incident intensity $\tilde{I}$ for a film with $n_s/n_n = 1/50$, $S_0 = 0.615$, $J = 5$ and $A = 1/6$. Once again we see that the plot is non-monotonic, but in the current case the curve has kinks at around $\tilde{I} = 5$ and $\tilde{I} = 11$. The maximum contraction is now larger, approximately $\lambda \approx 0.72$, i.e. we recover
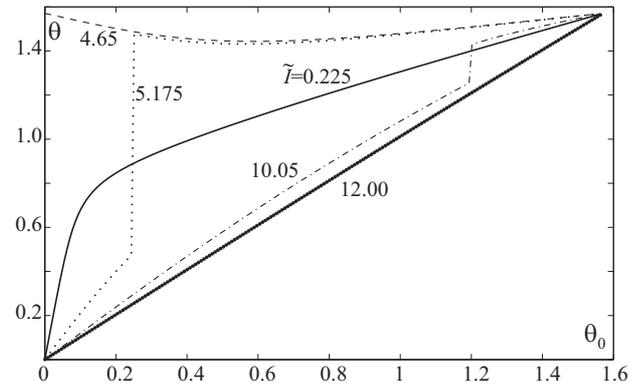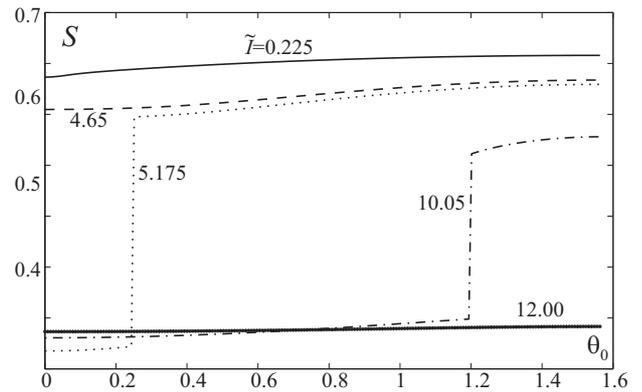
roughly two thirds of the thermal contraction of a simple monodomain system. Furthermore at larger intensities the deformation λ is very close to unity, i.e. there is almost no mechanical response for large intensities. Figs. 7 and 8 show the new orientation θ and order parameter S as functions of the initial orientation for several intensities.

At $\tilde{I} = 0.225$ there is very little reduction in the local order parameters, but rotations of directors away from $\underline{E}$ are quite large. One would expect this; since $\tilde{\mu}$ is much smaller the elastic resistance to rotation is now relatively smaller compared with the nematic imperative to rotate. The order parameter has not yet changed much; once again it has increased for a small range of angles around $\theta_0 = \pi/2$.

By $\tilde{I} = 4.65$ all domains are close to $\pi/2$, i.e. rotations are very large for those domains initially close to $\theta_0 = 0$. Since all domains are now close to $\pi/2$ contraction along $\underline{E}$ owing to rotation is essentially complete. Increasing $\tilde{I}$ then results in an increase in λ as the local order parameters become increasingly depressed.

Increasing the intensity to $\tilde{I} = 5.175$, which is above

the first kink in $\lambda(\tilde{I})$, we see interesting behavior in both the orientation and the order parameter of the domains. Domains initially close to θ_0 which had rotated to $\theta \sim \pi/2$ have now rotated back towards a cone close to $\underline{E}$. Since they are closer to $\underline{E}$, the majority of the photo-nematogens are in their *cis* state and thus domains within this cone have small order parameters. The domains which remain close to $\pi/2$ manage to maintain reasonably large order parameters, but they do reduce, and this reduction combined with the rotations mentioned drives the deformation rapidly back towards $\lambda = 1$. The first kink in fig 6 is the point where these back rotations begin.

As $\tilde{I}$ is increased further the cone widens, more domains rotate back towards their initial orientations $\theta \sim \theta_0$. Thus at $\tilde{I} = 10.05$ most domains have reverted to being close to their initial orientation and have small order parameters. There is still a narrow band of domains close to $\pi/2$ and the order parameters of domains within this band remain somewhat larger. The second kink in fig 6 occurs when back rotation is complete, and beyond this point one has $\theta \sim \theta_0$ for all domains. This is the case by $\tilde{I} = 12$. The order parameter for domains is now small for all θ_0, the system is essentially isotropic, there is no preferred direction, and the elastomer returns to $\lambda = 1$.

B.   Incident unpolarized light

We now consider *unpolarized* light incident normally upon a sample, that is we consider light traveling along the beam direction $\underline{k}$ shown in fig **??**, the electric field vectors being uniformly distributed in the plane perpendicular to $\underline{k}$. The average $\left\langle (\underline{E} \cdot \underline{u})^2 \right\rangle = Tr \left[\left\langle \underline{E}\,\underline{E} \right\rangle_E \left\langle \underline{u}\,\underline{u} \right\rangle_u \right]$ must now be recalculated, we have $\left\langle \underline{E}\,\underline{E} \right\rangle_E = \frac{E^2}{2}(\underline{z}\,\underline{z} + \underline{y}\,\underline{y}) = \frac{E^2}{2}(\underline{\delta} - \underline{x}\,\underline{x})$, while $\left\langle \underline{u}\,\underline{u} \right\rangle_u = S\hat{\underline{n}}\,\hat{\underline{n}} + \frac{(1-S)}{3}\underline{\delta}$, and thus:

$$\left\langle (\underline{E} \cdot \underline{u})^2 \right\rangle = \frac{E^2}{3}\left[1 - SP_2(\cos\theta)\right], \qquad (20)$$

where $\cos\theta = \hat{\underline{n}}.\underline{x}$ - i.e. the angle θ is now that between the director $\hat{\underline{n}}$ and the $\underline{x}$ direction. The fraction of *cis* nematogens is therefore:

$$\phi(S, \theta, \tilde{I}) = A \frac{\tilde{I}\left[1 - SP_2(\cos\theta)\right]}{3 + \tilde{I}\left[1 - SP_2(\cos\theta)\right]}. \qquad (21)$$

We once again take the Taylor limit, that is we assume each domain suffers the same uniaxial deformation. The unique direction is now the beam direction, thus we adopt the second of the deformation gradient tensors in eqn (18).

The step length tensors $\underline{l}_0$ and $\underline{l}^{-1}$ are given by eqns (13-17). Since the deformation gradient is isotropic within the yz plane domains which make the same polar angle with respect to the direction $\underline{k}$ but have different azimuthal angles within the yz plane are mechanically equivalent.

Our model predicts uniaxial extensions along the beam direction $\underline{k}$, fig **??**, and corresponding contractions in the plane of the film. Now the regions with director in the plane of the sample rotate away from the yz plane causing elongations along the beam direction in complete analogy with the effects described above. Such distortions turn out to be large in our model, i.e. comparable to those suffered by cooling monodomains. Figure 9 shows the equilibrium deformation gradient λ as a function of $\tilde{I}$ for the strongly cross-linked case $\tilde{\mu} = 1/10$. Figure 10 shows
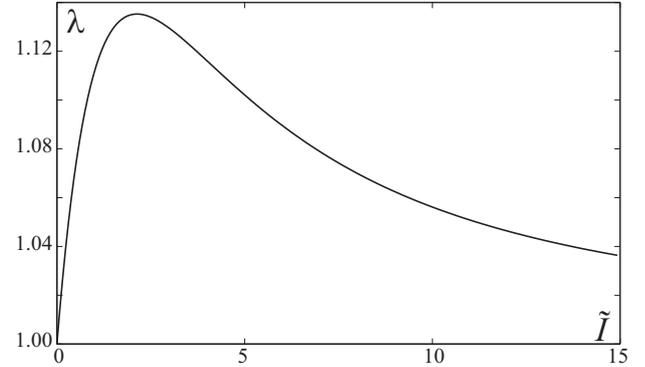

FIG. 9: The deformation λ along the beam propagation direction **k** as a function of the reduced intensity $\tilde{I}$ of unpolarized light on an elastomer with $\tilde{\mu} = 1/10$.

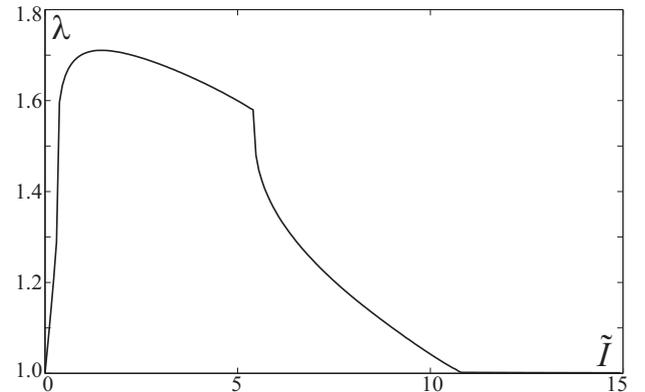the result for the weakly cross-linked case $\tilde{\mu} = 1/50$. In

FIG. 10: The in-plane contraction λ as a function of the reduced intensity $\tilde{I}$ of unpolarized light on an elastomer with $\tilde{\mu} = 1/50$.

both cases we observe that the deformation $\lambda > 1$, thus the film expands along the direction of light propagation and contracts by $1/\sqrt{\lambda}$ in the yz plane. The mechanical response for the weakly cross-linked case is somewhat larger – as before, rotations away from the electric field are bigger, leading to larger mechanical responses. The form and features of these plots are readily explained by the discussion in the previous section, in particular by considering the $\theta(\theta_0)$ and $S(\theta_0)$ relations at each $\tilde{I}$.
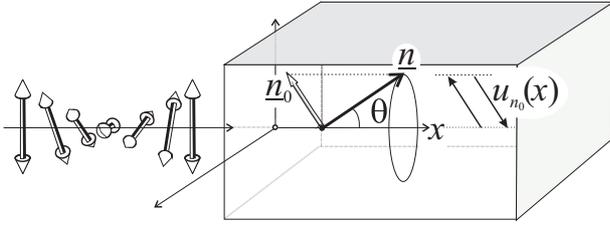
FIG. 11: The helical director distribution for a simple cholesteric (left). Initial directors are in the plane perpendicular to x, the helix axis. Directors are induced to rotate out of the transverse plane towards the helix axis, remaining in the $\underline{n}_0 - x$ plane. A shear displacement u in the $\underline{n}_0$ direction varies with x. (right).

This analysis of unpolarized light may also be relevant in polarized illumination but where scattering induces depolarization through a thick sample.

That the response to unpolarized light is larger than that to polarized light can be justified on purely geometrical grounds: the $\hat{n}_0$ vectors are uniformly distributed on the unit sphere. The polar axis is now $\underline{k}$ rather than $\underline{E}$. Being distributed with weight $\sin\theta_0 d\theta_0$, the majority of the $\hat{n}_0$ and thus the rods associated with the domains are in the equatorial region. The dye units are accordingly most susceptible to the $\underline{E}$ vectors of the unpolarized light, rather than formerly where the $\underline{E}$ vector was uniquely along the polar axis of the distribution of directors. We now turn to an even more extreme case of directors initially localized to an equatorial region:

C.   Unpolarized light incident on a cholesteric photo-elastomer

Consider a planar distribution of directors, all of which are in the yz plane, figure 11 (left). This is essentially the 2D equivalent of a standard polydomain. Practically, such a distribution could be realized using a cholesteric LCE with the helix axis parallel to the propagation direction of the incident unpolarized light. If the sample is thick compared with the pitch, one can adopt a coarse graining procedure. Variations over the length of the pitch can be integrated over and one is left with an effectively planar distribution of directors that would be uniformly illuminated by unpolarized light. The unique direction of the sample is then parallel to the propagation direction. Care is needed with this argument if the incident light is of wavelength at or close to the stop gap of the cholesteric. Then the component of incident light of the same circular handedness as that of the LCE is rejected by Bragg reflection (giving the characteristic colors of a cholesteric). The other handedness will penetrate and may behave as envisaged in the coarse-grained picture. The photonics of cholesterics is very subtle and absorption adds still further complications [29] that reveal our picture above is a simplification. Cholesterics

often have pitch in the visible part of the spectrum, that is their pitch is in the range $\sim 400-600$nm. The nematic polydomain films used by Ikeda [6] were 7μm thick; this would give for an equivalent cholesteric sample ~ 15 full rotations of the helix through the sample. For our model thus far to be applicable one must be careful to make sure that while the sample is thick compared with the pitch of the cholesteric, it is thin compared with the absorption length of the film, which can be tuned by reducing the concentration of dye in the film, or illuminating with light that isn't quite on resonance for the $trans \rightarrow cis$ isomerization. Since all domains are oriented initially in-plane (i.e. $\theta_0 = \pi/2$ for all domains) we no longer need to integrate over the initial orientation of domains.

Figure 11 (right) shows how the director can rotate towards the helix axis, moving in the plane of the original director and this axis. The plane in which $\hat{n}$ rotates itself rotates with advancing x. There are now more strain possibilities than before. The deformation gradient tensor $\underline{\underline{\lambda}}_k$, eqn (18), can be augmented by λ_{zx} and λ_{yx} shears associated with the displacements u in the transverse plane shown in the figure. Such a shear is advantageous since there is elongation along the diagonal of the $\hat{n}_0$-x plane section of the sample which accommodates the rotating director and its associated elongation. The possibility of tilted (or conical) cholesteric elastomer phases with associated shears is explored in the context of changing order parameter near the thermal cholesteric-isotropic phase transition [30, 31]. The spatially varying strain introduced is still compatible: the deformation gradient element λ_{ij} is $\partial R_i/\partial R_j^0$ where $\underline{R}$ and $\underline{R}_0$ are material positions in the target and reference states respectively. Clearly the second derivative of position must obey $\partial\lambda_{ij}/\partial R_k^0 = \partial\lambda_{ik}/\partial R_j^0$ which is here trivially satisfied since the variation is in the x direction – we are dealing with $\partial\lambda_{ix}/\partial x$ where $i = z, y$. The balance between z and y displacements and hence components of shear is best handled by taking coordinates based on z, that is locally taking $\hat{n}_0$ along z. For clarity in this context we denote the in-plane direction of $\hat{n}_0$ by the vector $\underline{m}$. A frame-independent method of writing this deformation is[31]:

$$\underline{\underline{\lambda}} = \left(\lambda - 1/\sqrt{\lambda}\right)\underline{x}\,\underline{x} + 1/\sqrt{\lambda}\underline{\underline{\delta}} + \lambda_{mx}\underline{m}\,\underline{x}. \qquad (22)$$

The free energy density (reduced by $n_n k_{\mathrm{B}}T$) to be minimized is again that of (19), but with the uniaxial elongation $\underline{\lambda}$ augmented by shear as above, and with ϕ given by eqn $\overline{(2}1)$. The equilibrium deformation adopted is given firstly by minimizing with respect to both λ_{mx} and λ. Details are similar to those of [31] but with the difference that there $S_0 = 0$ and that care with prefactors in the free energy has to be taken in comparing with here. As in [31] the optimal shear, given λ and θ is:

$$\lambda_{mx} = \frac{(r-1)sc}{r-(r-1)s^2}\lambda \qquad (23)$$

where r is shorthand for the anisotropy $l_\parallel/l_\perp$, and anal-

ogously for r_0, and where s denotes $\sin\theta$ and c is $\cos\theta$. The various l factors are given in eqns (15-17). Returning this shear to the elastic part of the free energy one then minimizes this part over λ and obtains:

$$\lambda_{eq}^3 = \frac{1}{2r}\left(r - (r-1)s^2\right)\left(r(r_0+1) - r_0(r-1)s^2\right) \quad (24)$$

Returning this λ to the elastic free energy gives the scaled energy:

$$f_{EL} = \tfrac{1}{2}\tilde{\mu}\frac{l_\perp^0}{l_\perp}\frac{3}{2^{2/3}r^{2/3}}\left[\frac{\left(r(r_0+1) - r_0(r-1)s^2\right)^2}{r - (r-1)s^2}\right].$$
$$(25)$$

In this free energy we have neglected the effects of Frank elasticity. Departure from transverseness of the director means that twist is reduced from its natural value that attains before deformation, and thus a Frank penalty arises. In many cholesteric elastomer problems Frank energy seems to be important and experiment will determine whether the current problem in the weak crosslinking limit should be revisited.

We can place limits on the magnitude of the deformation achieved. The largest deformation will occur if the domains rotate such that they are parallel to the x-axis, i.e $s = 0$, $c = 1$ and that response will be maximized if the rotation occurs without reducing the order parameter, i.e. when one rotates a still-elongated system. Taking $S = S_0$ for $l_\parallel$ and $l_\perp$ in (24) gives a $\lambda_1^3 = \tfrac{1}{2}r_0(r_0+1)$, that is:

$$\lambda_1 = \left[\frac{1}{2}\left(\frac{1+2S_0}{1-S_0}\right)\left(\frac{2+S_0}{1-S_0}\right)\right]^{\frac{1}{3}}. \quad (26)$$

For $S_0 = 0.615$ this yields $\lambda_1 = 2.7$, a significant expansion. Indeed λ_1 is greater than the elongation λ_r associated with the rotation of a monodomain by 90deg at constant order parameter. This apparently paradoxical situation arises because here the perpendicular contractions are forced to be equal by our (Taylor) assumption about polydomain response. The perpendicular strains are not optimal for any of the rotating domains and hence the elastomer is squeezed out along the cholesteric helical axis.

We can also predict the high intensity value of λ_{eq}. At high intensities ϕ from eqn (21) loses any angular dependence. The elastic energy (25) can be simply minimized over θ where it appears explicitly since there is no hidden θ dependence in S from ϕ in r. The result is $\theta = \theta_0 = \pi/2$. Setting $s = 1$ in eqn (24) then shows that λ in the high intensity limit is $\lambda_2 = [(r_0+r)/(2r)]^{1/3}$. The high intensity response falls in the interval $\lambda_2 = 1$ for $r = r_0$ corresponding to temperatures and fractions A low enough that high intensities have little effect on order, to $\lambda_2 = [(r_0+1)/2]^{1/3}$ where the intensity is sufficient to convert all domains to the isotropic state. Thus a bound on the high intensity value of the deformation
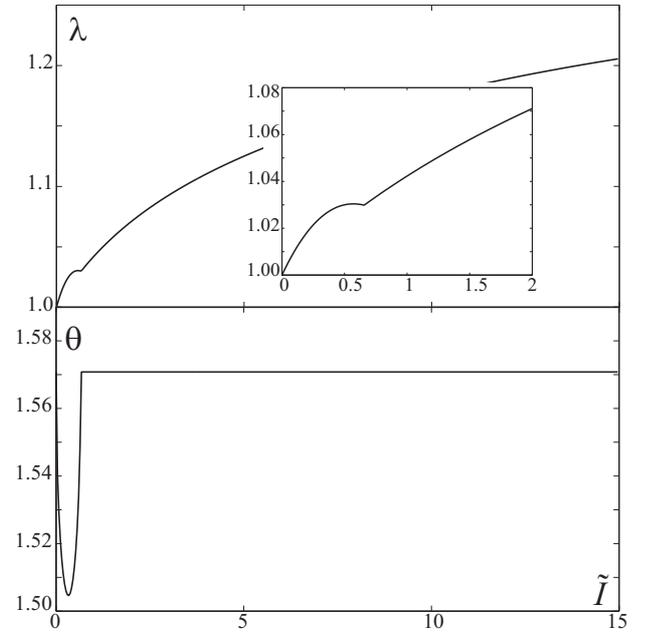

FIG. 12: Upper: The elongation along the helical axis for a cholesteric elastomer of $\tilde{\mu} = 1/10$ illuminated with unpolarized light of intensity $\tilde{I}$. Lower: The associated rotation of the director away from the yz plane.

gradient is λ_2, given by:

$$\lambda_2 = \left[\frac{1}{2}\left(\frac{2+S_0}{1-S_0}\right)\right]^{\frac{1}{3}}. \quad (27)$$

For $S_0 = 0.615$ this gives $\lambda_2 = 1.5$.

The response of cholesteric photo elastomers also depends on whether they are strongly or weakly crosslinked. The deformation and director rotation of a strongly linked network ($\tilde{\mu} = 1/10$) as a function of incident intensity are shown in figure 12. The variation of domain orientation and order parameter is the same for all domains since they all start with polar angle $\pi/2$ with respect to the propagation direction. Elongation along the helix axis initially increases, with domains departing briefly and weakly from the yz plane. The twist energy does not change much and the neglect of Frank effects is certainly appropriate. On the return of directors to the yz plane, the elongation thereafter increases more slowly and monotonically. Going to significantly larger intensities than is shown in the plot, the deformation asymptotes towards λ_2. Through the same interval of intensity, the order parameter of the domains decreases slowly from the initial value $S = 0.61$ to $S \sim 0.3$.

The situation is significantly different if we increase the number of nematogens per network strand. Figure 13 shows the elongation, director orientation and order as functions of $\tilde{I}$ for $\tilde{\mu} = 1/50$. Initially elongation is very rapid, associated with rapid director rotation with only slow reduction in the order parameter. Very soon there is a jump in elongation to close to the maximal possible elongation λ_1, upper dashed line in the elongation
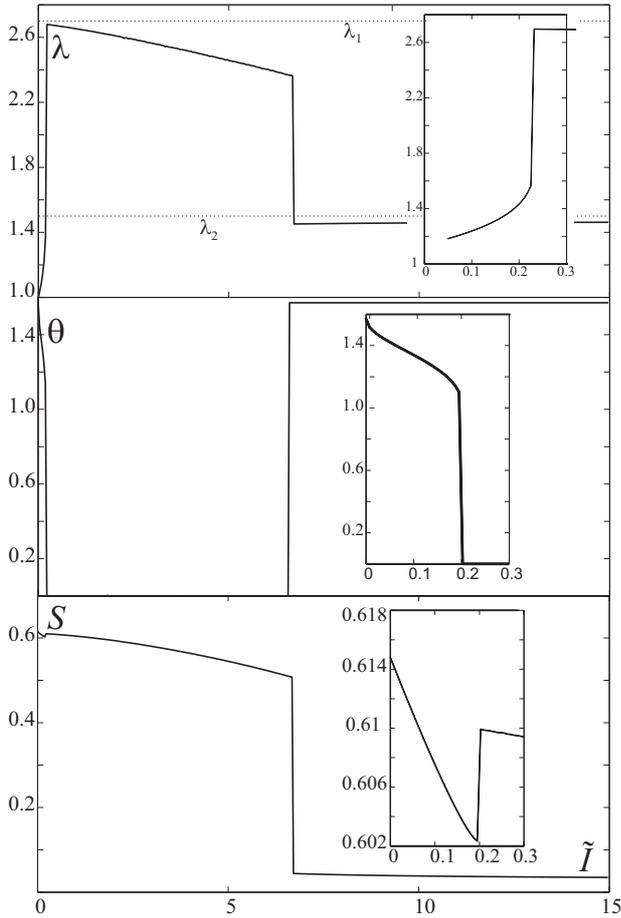
FIG. 13: Upper: Elongation λ for a cholesteric elastomer with $\tilde{\mu} = 1/50$ illuminated by light of reduced intensity $\tilde{I}$. Middle: Director angle θ. Lower: Order parameter S. Insets show the rapid variation and jumps at low intensities.

figure, the failure to attain the maximum being because the order parameter is very slightly reduced already. The jump is because of the jump in the director (see inset to the middle figure) away from the transverse plane to being along the helix axis. Twist is eliminated. Because the jump is away from the electric vector, the order parameter recovers somewhat. At higher intensities around $\tilde{I} \sim 6.5$, because of the reduction in order parameter the directors rotate back to the transverse plane and there is a concomitant reduction in the order parameter since the directors are again close to the electric vector. The elongation is reduced to close to the high intensity limit λ_2, lower dashed line, which is then approached from below at high $\tilde{I}$.

IV.   SUMMARY AND CONCLUSIONS

We have modeled the response of nematic polydomain photo-elastomers to polarized and unpolarized light. Polarized light lead to contraction along the polarization direction, a very useful control of mechanics that has

been seen in experiments on both nematic glasses and elastomers. We draw a distinction between weakly crosslinked elastomers which display large director rotations and hence qualitatively differing regions of mechanical response, and strongly linked systems where rotations are inhibited by the network and where responses, while still large, are not so big as in the weak case. We predict that larger responses are achieved for the same elastomer if they are irradiated with unpolarized light. Now the uniaxial axis is one of elongation and is along the propagation direction. This configuration is of perhaps the greatest applicability. It has been proposed [17, 18] that localized structures can be optically written into films of photo-elastomer on rigid substrates. In particular it would be useful to have raised bumps or dips in the surface topography which would depend on an incident spot of light but not on the underlying director if it were in-plane. Polydomain systems that we have described offer this opportunity.

Finally we examined the potentially largest response, namely from a 2-D system of domains as realized in cholesteric photo-elastomers. The response predicted for cholesterics is complex. It is possible that the neglect of Frank effects and avoiding the Taylor approximation might modify these subtleties.

APPENDIX A: UNIVERSAL FUNCTION

The function $g_0(x) \equiv \partial \ln Z(x)/\partial x$ given below eqn (9) is explicitly:

$$g_0(x) = \frac{\int_0^1 dy \left(\frac{3}{2}y^2 - \frac{1}{2}\right) \exp\left\{\frac{3}{2}y^2 x\right\}}{\int_0^1 dy \exp\left\{\frac{3}{2}y^2 x\right\}}$$

$$= -\frac{1}{2} - \frac{1}{2x} + \frac{1}{2x}\sqrt{\frac{3x}{2}} \frac{\exp\left(\frac{3x}{2}\right)}{\int_0^{\sqrt{\frac{3x}{2}}} \exp(y^2) dy}, \quad \text{(A1)}$$

the latter being for $x > 0$. It can be further simplified by rewriting the final term as $\mathcal{F}(x)$, defined by:

$$\mathcal{F}(x) = \frac{1}{2x} \frac{2\exp(3x/2)}{\sqrt{\pi}} \frac{\sqrt{3x/2}}{\mathrm{erfi}(\sqrt{3x/2})}, \quad \text{(A2)}$$

where $\mathrm{erfi}(y)$ is the imaginary error function [32]. Thus:

$$g_0(x) = -\frac{1}{2} - \frac{1}{2x} + \mathcal{F}(x). \quad \text{(A3)}$$

One can extend this result for $x < 0$ using analytic continuation on the function $\mathcal{F}(x)$ for imaginary arguments. Many routines exist for numerically calculating
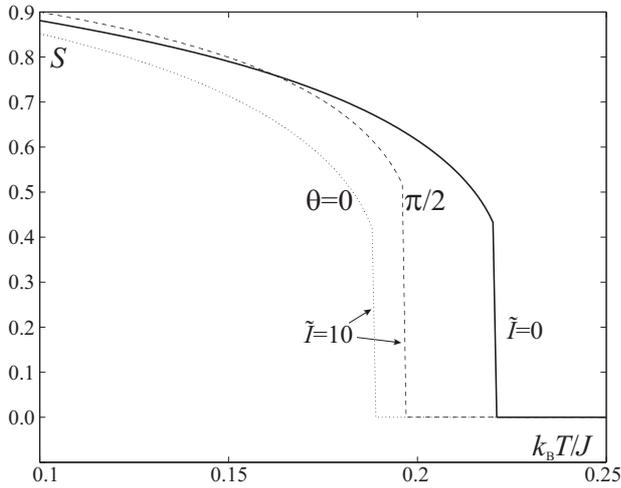
FIG. 14: The equilibrium order parameter S as a function of $k_B T/J$ within the standard Maier-Saupe model, and within our modified version for domains illuminated with polarized light of intensity $\tilde{I} = 10$ aligned both parallel and perpendicular to the electric field $\underline{E}$.

the imaginary error function quickly and accurately. For $x \to -\infty$ the function g_0 tends towards -0.5 while for $x \to \infty$ it tends towards 1. It has the sigmoid shape required to yield a first order phase transition applying self-consistency graphically.

The inverse function $g_0^{-1}(S)$ can easily be achieved numerically and gives us the mean field $h = k_B T g_0^{-1}(S)$ as a function of the order parameter S. Finally it is trivial to show that the partition function $Z_0(h/k_B T)$ can be written as a function of S and is given by:

$$Z_0(S) = \frac{\exp(g_0^{-1}(S))}{1 + g_0^{-1}(S)(1 + 2S)}, \qquad (A4)$$

thus all terms in the Maier-Saupe free energy involving the mean field h within the nematic free energy can be re-written as explicit functions of the order parameter S.

APPENDIX B: VARIATION OF NEMATIC ORDER WITH TEMPERATURE AND ILLUMINATION

The equilibrium order parameter S obtained by minimizing this free energy is plotted as a function of $k_B T/J$ in figure 14 for several interesting cases. Firstly the plot for $\tilde{I} = 0$ simply gives the standard Maier-Saupe result, whereby there is a first-order phase transition from a low temperature nematic phase ($S > 0$) to a high temperature isotropic phase ($S = 0$). The transition occurs at $k_B T_{NI}/J = 0.22$, and at this point the value of the order parameter in the nematic phase is $S = 0.43$. Also shown are plots for a relatively high intensity $\tilde{I} = 10$, both for a domain with director along $\underline{E}$ ($\theta = 0$) and perpendicular to $\underline{E}$ ($\theta = \pi/2$). In both these latter cases we have

taken the fraction of nematogens that are photo-active $A = 1/6$. It is interesting to note that for both of these plots the apparent nematic-isotropic transition temperature T_{NI} has reduced. Furthermore T_{NI} is lower for domains oriented with the field rather than perpendicular to it. Finally we note that for sufficiently small values of $k_B T/J$ illumination of domains perpendicular to $\underline{E}$ results in an increase in the order parameter relative to the standard Maier-Saupe result. The order parameter S is an average over the *trans* and photo-inert nematogens only. For a domain with director perpendicular to the field, nematogens perpendicular to the director and along the field serve to lower S. Illumination preferentially removes these nematogens, thus increasing S. One can also define a bulk order parameter $Q = (1 - \phi)S$ which takes into account the reduced number of nematogens contributing, and within our model this parameter is always smaller than the canonical Maier-Saupe result. The bulk order parameter Q is the value measured by bi-refringence. By contrast NMR measures the order S of the nematic species. It is interesting to note that the transformation $Q = (1 - \phi)S$ renders eqn (11) back into the usual MS form.

APPENDIX C: THE DEPLETED FREELY JOINTED ROD MODEL

The freely jointed rod model gives a simple connection between the step-length tensor and the order parameter tensor $\underline{\underline{S}}$. For the initial tensor $\underline{\underline{l}}_0$ we assume that the polymer chain between cross-links consists of rods of length a connected to each other by flexible joints, i.e. there is no coupling between the orientation of one rod and its neighbours. The span vector is given by $\underline{R}_0 = \sum_{i=1}^{N} \underline{a}_i$ where $\underline{a}_i$ is a vector of magnitude a pointing along the direction of the ith rod. The step-length tensor $\underline{\underline{l}}_0$ is given by:

$$\underline{\underline{l}}_0 = \frac{3 \langle \underline{R}_0 \underline{R}_0 \rangle}{Na}. \qquad (C1)$$

Inserting the above form for $\underline{R}_0$ into eqn (C1), we obtain:

$$\underline{\underline{l}}_0 = \frac{3a^2 N \langle \hat{\underline{a}}\,\hat{\underline{a}} \rangle}{Na} = a(\underline{\underline{\delta}} + 2\underline{\underline{S}}), \qquad (C2)$$

where we have used eqn (2) to replace the average $\langle \hat{\underline{a}}\,\hat{\underline{a}} \rangle$. Assuming $\underline{\underline{S}}$ is uniaxial about a director $\hat{n}_0$ with scalar order parameter S_0, and using eqn (2), gives:

$$\underline{\underline{l}}_0 = a(1 - S_0)\left[\frac{3S_0}{1 - S_0}\hat{n}_0\,\hat{n}_0 + \underline{\underline{\delta}} \right] \qquad (C3)$$

The current step-length tensor $\underline{\underline{l}}$ has a slightly more complicated form than the original value $\underline{\underline{l}}_0$ since when rods bend, not only do they cause a change in the local order parameter, but they also change their step

length. We assume the fraction of nematogens in the *cis* state is ϕ, thus the fraction of *trans* or simply photo-inert rods is $(1 - \phi)$. As above, we model the polymer chain between two cross-links as a random walk, however the chain now consists of two different monomers, the *trans*/photo-inert rods described by a vector $\underline{a}$ and the *cis* rods described by a vector $\underline{b}$. The span vector of the chain is now given by $\underline{R} = \sum_{i=1}^{(1-\phi)N} \underline{a}_i + \sum_{j=1}^{\phi N} \underline{b}_j$, where N is the number of monomers between the cross-links. The *cis* molecules are assumed to be be isotropically disposed, thus $\langle \underline{b}_i \underline{b}_j \rangle = (b^2/3)\underline{\underline{\delta}}\delta_{ij}$, while the *trans*/photo-inert rods are uniaxially ordered, thus $\langle \underline{a}_i \underline{a}_j \rangle = (a^2/3)\delta_{ij}(\underline{\underline{\delta}} + 2\underline{\underline{S}})$. Evaluating the average $\langle \underline{R}\,\underline{R} \rangle = (1 - \phi)N(a^2/3)(\underline{\underline{\delta}} + 2\underline{\underline{S}}) + \phi N(b^2/3)\underline{\underline{\delta}}$. Extracting a factor of Na (the arc length for the unirradiated polymer that was extracted in defining $\underline{\underline{l}}_0$ in (C1)), the current step-length tensor is then given by:

$$\underline{\underline{l}} = a\left[(1 - \phi)\left\{ (1 - S)\underline{\underline{\delta}} + 3S\hat{n}\,\hat{n} \right\} + \phi(b/a)^2\underline{\underline{\delta}} \right] \quad \text{(C4)}$$

where we have substituted for $\underline{\underline{S}}$ from eqn (2) assuming a uniaxial form. The forms of the various step lengths l given in the text can be read off either from eqn (C3) or from (C4). Finally in calculations we require the inverse of the current step-length tensor, that is $\underline{\underline{l}}^{-1}$. Inverting eqn (C4) then gives:

$$\underline{\underline{l}}^{-1} = \frac{1}{a\left[(1 - \phi)(1 - S) + \phi(b/a)^2\right]} \times \left[\frac{-3S(1 - \phi)}{(1 + 2S)(1 - \phi) + \phi(b/a)^2}\hat{n}\,\hat{n} + \underline{\underline{\delta}} \right]. \quad \text{(C5)}$$

Only if $\phi = 0$ does (C5) become a standard $\underline{\underline{l}}^{-1}$.

[1] H. Finkelmann, E. Nishikawa, G. G. Pereira, and M. Warner, Phys. Rev. Lett **87**, 015501 (2001).

[2] P. M. Hogan, A. R. Tajbakhsh, and E. M. Terentjev, Phys. Rev. E **65**, 041720 (2002).

[3] M.-H. Li, P. Keller, B. Li, X. Wang, and M. Brunet, Adv. Mat. **15**, 569 (2003).

[4] M. Camacho-Lopez, H. Finkelmann, P. Palffy-Muhoray, and M. Shelley, Nature Mater. **3**, 307 (2004).

[5] T. Ikeda, M. Nakano, Y. Yu, O. Tsutsumi, and A. Kanazawa, Adv. Matter. **15**, 201 (2003).

[6] Y. Yu, M. Nakano, and T. Ikeda, Nature **425**, 145 (2003).

[7] K. D. Harris, R. Cuypers, P. Scheibe, C. L. van Oosten, C. W. M. Bastiaansen, J. Lubb, and D. J. Broer, J. Mat. Chem. **15**, 5043 (2005).

[8] G. N. Mol, K. D. Harris, C. W. M. Bastiaansen, and D. J. Broer, Adv. Funct. Mat. **15**, 1155 (2005).

[9] N. Tabiryan, S. Serak, X.-M. Dai, and T. Bunning, Optics Express **13**, 7442 (2005).

[10] H. Finkelmann and H. Wermter, ACS Abstracts **219**, 189 (2000).

[11] A. Tajbakhsh and E. Terentjev, Eur. Phys. J. E **6**, 181 (2001).

[12] I. Kundler and H. Finkelmann, Macromol. Chem. Rap. Commun. **16**, 679 (1995).

[13] J. Küpfer and H. Finkelmann, Macromol. Chem. Phys. **195**, 1353 (1994).

[14] C. L. M. Harvey and E. M. Terentjev, Eur. Phys. J. E **23**, 185 (2007).

[15] K. K. Hon, D. Corbett, and E. M. Terentjev, Eur. Phys. J. E **25(1)**, 83 (2008).

[16] A. W. Broerman, D. C. Venerus, and J. D. Schieber, J. Chem. Phys. **111**, 6965 (1999).

[17] M. Warner and L. Mahadevan, Phys. Rev. Lett. **92**, 134302 (2004).

[18] Z. Y. Wei and L. H. He, J. Chem. Phys. **124**, 064708 (2006).

[19] M.-H. Li, P. Keller, J. Yang, and P.-A. Albouy, Adv. Mat. **16**, 1922 (2004).

[20] D. Corbett and M. Warner, Phys. Rev. Lett **96**, 237802 (2006).

[21] C. D. Eisenbach, Makromol. Chem. **179**, 2489 (1978).

[22] F. Serra and E. M. Terentjev, J. Chem. Phys. **128**, 224510 (2008).

[23] W. Maier and A. Saupe, Z. Naturforsch **14a**, 882 (1959).

[24] P. Bladon, E. M. Terentjev, and M. Warner, Phys. Rev. E **47**, R3838 (1993).

[25] M. Warner and E. M. Terentjev, *Liquid Crystal Elastomers* (revised paperback edition, OUP, Oxford, 2007).

[26] A. Greve, H. Finkelmann, and M. Warner, Eur. J. Phys. E **5**, 281 (2001).

[27] G. Feio, J. L. Figueirinhas, A. R. Tajbakhsh, and E. M. Terentjev, Phys. Rev **B78**, 020201(R) (2008).

[28] F. Elias, S. Clarke, R. Peck, and E. Terentjev, Europhys. Lett. **47**, 442 (1999).

[29] J. Nehring, J. Chem. Phys. **75**, 4326 (1981).

[30] R. A. Pelcovits and R. B. Meyer, Phys. Rev. E **66**, 031706 (2002).

[31] M. Warner and E. M. Terentjev, Macromol. Symp. **200**, 81 (2003).

[32] http://mathworld.wolfram.com/Erfi.html.